

Accretion process onto super-spinning objects

Cosimo Bambi^{1,*} Katherine Freese^{2,†} Tomohiro Harada^{3,‡} Rohta Takahashi^{4,§} and Naoki Yoshida^{1,¶}

¹*Institute for the Physics and Mathematics of the Universe,
The University of Tokyo, Kashiwa, Chiba 277-8568, Japan*

²*The Michigan Center for Theoretical Physics, Department of Physics,
University of Michigan, Ann Arbor, Michigan 48109, USA*

³*Department of Physics, Rikkyo University, Toshima, Tokyo 171-8501, Japan*

⁴*Cosmic Radiation Laboratory, the Institute of Physical and Chemical Research, Wako, Saitama 351-0198, Japan*

(Dated: October 7, 2018)

The accretion process onto spinning objects in Kerr spacetimes is studied with numerical simulations. Our results show that accretion onto compact objects with Kerr parameter (characterizing the spin) $|a| < M$ and $|a| > M$ is very different. In the super-spinning case, for $|a|$ moderately larger than M , the accretion onto the central object is extremely suppressed due to a repulsive force at short distance. The accreting matter cannot reach the central object, but instead is accumulated around it, forming a high density cloud that continues to grow. The radiation emitted in the accretion process will be harder and more intense than the one coming from standard black holes; e.g. γ -rays could be produced as seen in some observations. Gravitational collapse of this cloud might even give rise to violent bursts. As $|a|$ increases, a larger amount of accreting matter reaches the central object and the growth of the cloud becomes less efficient. Our simulations find that a quasi-steady state of the accretion process exists for $|a|/M \gtrsim 1.4$, independently of the mass accretion rate at large radii. For such high values of the Kerr parameter, the accreting matter forms a thin disk at very small radii. We provide some analytical arguments to strengthen the numerical results; in particular, we estimate the radius where the gravitational force changes from attractive to repulsive and the critical value $|a|/M \approx 1.4$ separating the two qualitatively different regimes of accretion. We briefly discuss the observational signatures which could be used to look for such exotic objects in the Galaxy and/or in the Universe.

PACS numbers: 04.20.Dw, 97.60.-s, 95.30.Lz, 97.10.Gz

I. INTRODUCTION

It is widely believed that the final product of the gravitational collapse of matter is a black hole (BH). In classical general relativity (GR), astrophysical BHs should be completely characterized by just three parameters: the mass M , the charge Q , and the spin J . In this paper we focus on chargeless BHs. The spin is often replaced by the Kerr parameter $a = J/M$. In classical GR, the values of M and a cannot be completely arbitrary, as they must satisfy the relation $|a| < M$, which is the condition for the existence of the horizon. To see this we can examine the 3+1 dimensional Kerr solution. The position of the horizon is given by the expression [1, 2]

$$r_H = M + \sqrt{M^2 - a^2}. \quad (1)$$

It is clear that in (3+1)D spacetime the horizon cannot be formed if

$$M < |a|. \quad (2)$$

In the absence of a horizon, there would be naked singularities which are not allowed in GR. Indeed, if condition (2) is fulfilled, the Kerr metric makes it possible to reach the physical singularity at $r = 0$ from some large r in finite time without crossing any horizon. One could thus consider closed time-like curves and violate causality (see e.g. section 66c of [3] or ref. [4]). For this reason, usually some kind of cosmic censorship is assumed and naked singularities are forbidden [5]. In particular, it is believed that naked singularities cannot be created by any physical process and therefore that the end-state of the gravitational collapse of matter is a Kerr BH with $|a| < M$ [5].

*Electronic address: cosimo.bambi@ipmu.jp

†Electronic address: ktfreese@umich.edu

‡Electronic address: harada@rikkyo.ac.jp

§Electronic address: rohta@riken.jp

¶Electronic address: naoki.yoshida@ipmu.jp

However, in this paper we consider objects which *do* violate the Kerr bound, i.e. with $|a| > M$. We call them “super-spinars”, as proposed in [6]: since they have no event horizon, by the standard definition they are not BHs. Our main motivation is simple. The singularity can be viewed as the place where new physics should be expected: here observer-independent quantities like the scalar curvature diverge, while GR presumably breaks down above the Planck scale. It is therefore not unreasonable to expect that causality is conserved, not because the collapsing matter can form only objects with $|a| < M$, but because actually the central singularity is replaced by some high curvature region due to some quantum gravity effects, see e.g. [6, 7]. In this case, there is apparently no reason to believe that the final product of the gravitational collapse of matter cannot have $|a| > M$. Another possibility is that the collapsing matter forms a super-compact star with $|a| > M$ and exotic equations of state: now there is no central singularity, since the Kerr metric is a solution of Einstein equations only in vacuum; matter could have very exotic equation of state once it reaches densities so high that our knowledge of physics becomes inadequate. Actually, in general the metric at very small radii may deviate from the Kerr solution (the uniqueness theorem does not hold in absence of a regular horizon [8]), but in our discussion we will neglect such a possibility.

In this paper, we extend the studies started in [9, 10]. The goal is to examine the main differences between the cases $|a| < M$ and $|a| > M$. Previous papers [9, 10] discussed implications on the apparent shape. There it was found that, even if the bound is violated by a small amount, the shadow cast by the super-spinar (i.e. how it blocks light coming to us from an object behind it) changes significantly from the case with $|a| < M$: the shadow for the super-spinar is about an order of magnitude smaller as well as distorted. This distinction can be used as an observational signature in the search for these objects. Based on recent observations at mm wavelength of the super-massive BH candidate at the Center of the Galaxy [11], the authors speculated on the possibility that it might violate the Kerr bound.

In this paper we discuss the process of accretion in a Kerr background with arbitrary value of the Kerr parameter. For $|a|$ moderately larger than M , we find that the accreting matter cannot reach the central object, but is accumulated around it, forming a high density cloud. That may have interesting observational consequences. First, because of the high density and the high temperature of the plasma, the radiation produced in the accretion process can be much harder and more intense than the one coming from BHs. Second, there might be violent phenomena like bursts, when the amount of accumulated gas is large enough to gravitationally collapse. For higher values of $|a|$, the cloud evolves into a sort of disk, which is however very different from the usual disk of accretion around a BH: here the disk extends from $r \approx M$ to the center, leading to rapid accretion, increasing efficiently the mass of the central object, and producing hard radiation at very small radii.

Unlike the case of Kerr BHs, we do not know if super-spinars are stable under small perturbations. Previous work has found that some very rapidly rotating objects in 3+1 and higher dimensions can be unstable [12, 13]. To address this point regarding the super-spinars studied in this paper, one should do a linearized analysis of the perturbations of these objects. However, the conclusion would be determined by the boundary conditions at the surface of super-spinars, which presumably depend on the quantum theory of gravity and are therefore unknown. Such a question cannot thus be addressed at present: here we just assume that super-spinars are stable and we study the accretion process onto these objects.

Conventions: We use natural units $G_N = c = k_B = 1$. The metric has signature $(- + + +)$.

II. MODEL AND ASSUMPTIONS

A. Equations

In this subsection we briefly review the basic ingredients of the formalism used in our study. For more details, see e.g. [14, 15, 16] and references therein.

We are going to simulate the accretion process of a test fluid in a background curved spacetime; that is, we neglect the back-reaction of the fluid to the geometry of the spacetime, as well as the increase in mass and the variation in spin of the central object due to accretion. Such an approximation is surely reasonable if we want to study a stellar mass compact object in a binary system, because in this case the matter captured from the stellar companion is typically small in comparison with the total mass of the compact object. The results of our simulations should not be applied to long-term accretion onto a super-massive object at the center of a galaxy, where accretion makes the mass of the compact object increase by a few orders of magnitude from its original value.

Our master formulas are the equations of conservation of baryon number and of the fluid energy-momentum tensor

$$\nabla_\mu J^\mu = 0, \quad (3)$$

$$\nabla_\mu T^{\mu\nu} = 0, \quad (4)$$

where J^μ and $T^{\mu\nu}$ are respectively the current of matter and the fluid energy-momentum tensor

$$J^\mu = \rho u^\mu, \quad (5)$$

$$T^{\mu\nu} = \rho h u^\mu u^\nu + p g^{\mu\nu}. \quad (6)$$

Here ρ is the rest-mass energy density (for example, in the case of hydrogen plasma, $\rho = n(m_p + m_e)$, where n is the number density of protons/electrons and m_p (m_e) the proton (electron) mass), p is the pressure, u^μ is the fluid four-velocity, $h = 1 + \epsilon + p/\rho$ is the specific enthalpy, and ϵ is the specific internal energy density. In other words, $\rho\epsilon$ is the thermal energy density ($\rho\epsilon = 3nT$ for non-relativistic hydrogen plasma), while $\rho(1 + \epsilon)$ is the total energy density of the fluid. In order to solve the system, an equation of state $p = p(\rho, \epsilon)$ must be specified.

In the 3+1 formalism, the line element of the spacetime is written in the form

$$ds^2 = -(\alpha^2 - \beta_i \beta^i) dt^2 + 2\beta_i dt dx^i + \gamma_{ij} dx^i dx^j, \quad (7)$$

where α is the lapse function, β^i the shift vector and γ_{ij} the 3-metric induced on each space-like slice. Greek indices run from 0 to 3 and are lowered (uppered) by the 4-metric $g_{\mu\nu}$ (inverse 4-metric $g^{\mu\nu}$). Latin indices run from 1 to 3 and are lowered (uppered) by the 3-metric γ_{ij} (inverse 3-metric γ^{ij}). For Eulerian observers, the 3-velocity of the fluid is given by

$$v^i = \frac{u^i}{\alpha u^0} + \frac{\beta^i}{\alpha}, \quad (8)$$

while the covariant components can be obtained by using γ_{ij} , i.e. $v_i = \gamma_{ij} v^j$. For what follows, it is convenient to use two sets of variables. The *primitive variables* are

$$\mathbf{V} = (\rho, v^i, p)^T \quad (9)$$

and are the quantities whose evolution and quasi-steady state (if any) we want to determine. The hydrodynamical equations are instead solved in term of the *conserved variables*

$$\mathbf{U} = (D, S_i, \tau)^T, \quad (10)$$

which can be written in term of the primitive ones as

$$D = \rho W, \quad (11)$$

$$S_i = \rho h W^2 v_i, \quad (12)$$

$$\tau = \rho h W^2 - D - p, \quad (13)$$

where $W = \alpha u^0 = (1 - v^2)^{-1/2}$ is the Lorentz factor and $v^2 = v_i v^i$. The equations of conservation (3) and (4) can now be written as

$$\frac{1}{\sqrt{-g}} \left[\frac{\partial}{\partial t} (\sqrt{\gamma} \mathbf{U}) + \frac{\partial}{\partial x^i} (\sqrt{-g} \mathbf{F}^i) \right] = \mathcal{S}, \quad (14)$$

where \mathbf{F}^i and \mathcal{S} are defined by [14]

$$\mathbf{F}^i = \left(D (v^i - \beta^i/\alpha), S_j (v^i - \beta^i/\alpha) + p \delta_j^i, \tau (v^i - \beta^i/\alpha) + p v^i \right)^T, \quad (15)$$

$$\mathcal{S} = \left(0, T^{\mu\nu} (\partial_\mu g_{\nu j} - \Gamma_{\mu\nu}^\lambda g_{\lambda j}), \alpha (T^{\mu 0} \partial_\mu \ln \alpha - T^{\mu\nu} \Gamma_{\mu\nu}^0) \right)^T. \quad (16)$$

These equations are solved numerically by integrating over the computational cells of the discretized spacetime.

B. Background metric and test fluid

In our study, the spacetime is described by the Kerr metric. Using the Boyer-Lindquist coordinates, the line element (7) becomes

$$ds^2 = -\alpha^2 dt^2 + \frac{\Sigma^2 \sin^2 \theta}{\varrho^2} (d\phi - \omega dt)^2 + \frac{\varrho^2}{\Delta} dr^2 + \varrho^2 d\theta^2, \quad (17)$$

where $\alpha^2 = \varrho^2 \Delta / \Sigma^2$, $\omega = 2aMr / \Sigma^2$, and Δ , ϱ^2 and Σ^2 are defined by

$$\Delta = r^2 - 2Mr + a^2, \quad (18)$$

$$\varrho^2 = r^2 + a^2 \cos^2 \theta, \quad (19)$$

$$\Sigma^2 = (r^2 + a^2)^2 - a^2 \Delta \sin^2 \theta. \quad (20)$$

The equation of state of the accreting matter is the one of an ideal gas with constant polytropic index Γ :

$$p = (\Gamma - 1) \epsilon \rho. \quad (21)$$

In the simulations, we take $\Gamma = 5/3$ (non-relativistic gas). The effects of electromagnetic fields on gas dynamics is neglected, as well as non-adiabatic phenomena, like viscosity or heat transfer.

C. Calculation method

Our calculations are made with the relativistic hydrodynamics (RHD) module of the public available code PLUTO [17, 18], properly modified for the case of curved spacetime, as described in subsection II A. We do not solve the Riemann problem to compute fluxes, but we use a Lax-Friedrichs scheme; flux contributions are evaluated from all directions simultaneously (no dimensional splitting); time evolution uses a second order Runge-Kutta algorithm.

The computational domain is the 2D axysymmetric space $r_{in} < r < 20 M$ and $0 < \theta < \pi$, where r_{in} is set according to the case under study. In this paper we present the results for six different values of the Kerr parameter: $a = 0.4 M$, $a = 0.9 M$, $a = 1.1 M$, $a = 1.4 M$, $a = 2.0 M$, and $a = 3.0 M$. In the first two cases, we have a BH with event horizon at radial coordinate $r_H = 1.92 M$ and $r_H = 1.44 M$ respectively, and the inner boundary is set just outside the event horizon: $r_{in} = 2.00 M$ for $a = 0.4 M$ and $r_{in} = 1.50 M$ for $a = 0.9 M$. We adopt free-outflow boundary conditions, i.e. we set zero gradient across the inner boundary:

$$\frac{\partial \rho}{\partial n} = \frac{\partial p}{\partial n} = \frac{\partial v^i}{\partial n} = 0, \quad (22)$$

where n is the coordinate orthogonal to the boundary plane.

For $|a| > M$, there is no event horizon but a naked singularity at $r = 0$. In the simulations presented in this paper, we took $r_{in} = 0.5 M$ and we imposed no flow from the boundary. The choice of the value of r_{in} can appear arbitrary. However, it does not significantly alter the final result for any value of $|a|/M$, while for smaller r_{in} the computational time increases considerably. As for the choice of the boundary condition, we have imposed no flow from the boundary, in order to prevent an unphysical injection of gas from the center.

Both for BHs and super-spinars, at the beginning of the simulations the density of the gas (plasma) around the compact objects is constant (and equal to ρ_0 , see below) and we start injecting gas from the outer boundary at a constant rate. The gas is injected with radial velocity $v_r = -0.0001$, while $v_\theta = v_\phi = 0$. We found that, for a given accretion rate, the final density profile is independent of the injection velocity for $v_r \lesssim -0.001$. Indeed, for small values of the injection velocity, the evolution of the gas is determined by the gravitational force and not by the initial conditions.

The unit of length (and time) is the parameter M :

$$M = 1.5 \cdot 10^6 \left(\frac{M}{10 M_\odot} \right) \text{ cm}, \quad (23)$$

while the unit of density, ρ_0 , is unspecified. The mass accretion rate of the system in the simulations is

$$\dot{M} = 3.4 \cdot 10^{17} \left(\frac{M}{10 M_\odot} \right)^2 \left(\frac{\rho_0}{10^{-3} \text{ g/cm}^3} \right) \text{ g/s}, \quad (24)$$

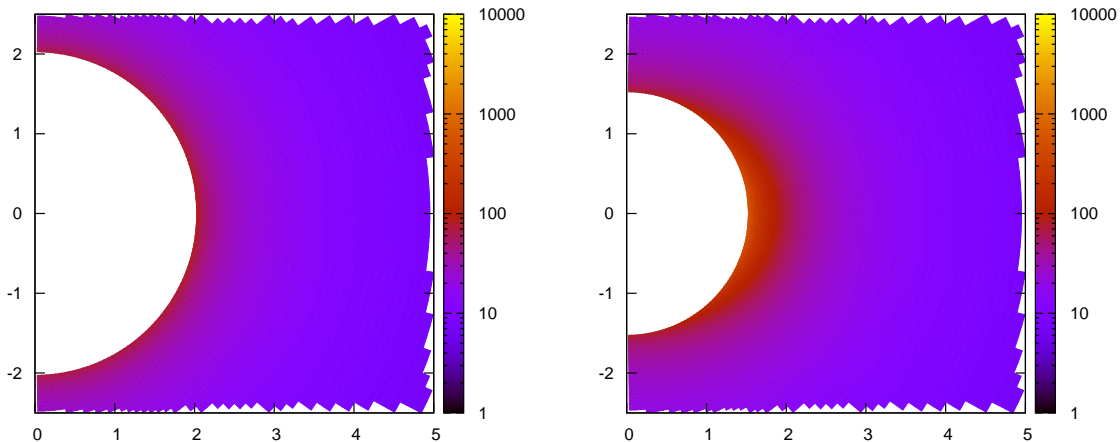


FIG. 1: Density of the accretion flow around a Kerr BH with $a = 0.4 M$ (left panel) and $a = 0.9 M$ (right panel). The inner boundary is at $r_{in} = 2.00 M$ for the case $a = 0.4 M$, and at $r_{in} = 1.50 M$ for the case $a = 0.9 M$. The unit of length along the x and y axes is M . The density scale (shown on the right side of each figure) ranges from ρ_0 to $10^4 \rho_0$, where ρ_0 is our unit of density (see discussion in subsection II C).

or, in Eddington units¹,

$$\left(\frac{\dot{M}}{\dot{M}_E}\right) = 0.24 \left(\frac{M}{10 M_\odot}\right) \left(\frac{\rho_0}{10^{-3} \text{ g/cm}^3}\right). \quad (25)$$

If we want to consider the accretion process onto an object with a certain mass at a particular accretion rate, we have to adjust the unit of density ρ_0 . For example, in the case of a super-massive object with $M = 10^6 M_\odot$ and accreting at 10^{-6} its Eddington limit, probably like the BH candidate at the Galactic Center, one has to take $\rho_0 = 10^{-13} \text{ g/cm}^3$.

Because of our simple treatment of the accreting matter, the gas temperature becomes extremely high. Here we simply impose a maximum temperature: this work does not aspire to get an accurate description of the accretion process, but only to figure out the main differences between the accretion process onto objects with $|a| < M$ and $|a| > M$. We have checked that the choice of T_{max} does not change significantly the final results: for $T_{max} = 10 \text{ KeV}$, 100 KeV and 1 MeV , the density changes by at most a few percent, while we do not expect that our simulations are as accurate.

III. RESULTS

A. Numerical study

The results of the simulations are summarized in figs. 1, 2, 3, 4, and 5. In fig. 1, we present the density, ρ , of the accretion flow onto BH with Kerr parameter $a = 0.4 M$ (left panel) and $a = 0.9 M$ (right panel). The density scale in these and the other pictures ranges from ρ_0 to $10^4 \rho_0$, where ρ_0 is our unit of density, as discussed in subsection II C. The white area is out of the domain of computation. For both choices of a , the accretion flow reaches a quasi-steady state, that is, the density does not depend on time.

Fig. 2 (left panel) shows the density of the accretion flow around a super-spiner with $a = 1.1 M$. We use the same color intensity scale of fig. 1, in order to facilitate the comparison between the cases $|a| < M$ and $|a| > M$. For the cells with density higher (lower) than $10^4 \rho_0$ (ρ_0), we use the same color scheme as though their density were $10^4 \rho_0$ (ρ_0). For example, a cell with $\rho = 10^6 \rho_0$ will have the same color as a cell with $\rho = 10^4 \rho_0$, and a cell with $\rho_0 = 10^{-6} \rho_0$ will have the same color as a cell with ρ_0 . As in the BH case, the white area is the region out of the

¹ Since we assume that the process is adiabatic, the unit of density ρ_0 can be left unspecified and our results can be applied (in principle) to any accretion rate, even orders of magnitude different. Such an assumption holds only for small accretion rates and optically thin gas. For example, our results would predict no qualitative differences between sub-Eddington and super-Eddington accretions, which is definitely not true because for high accretion rates the pressure of radiation cannot be neglected.

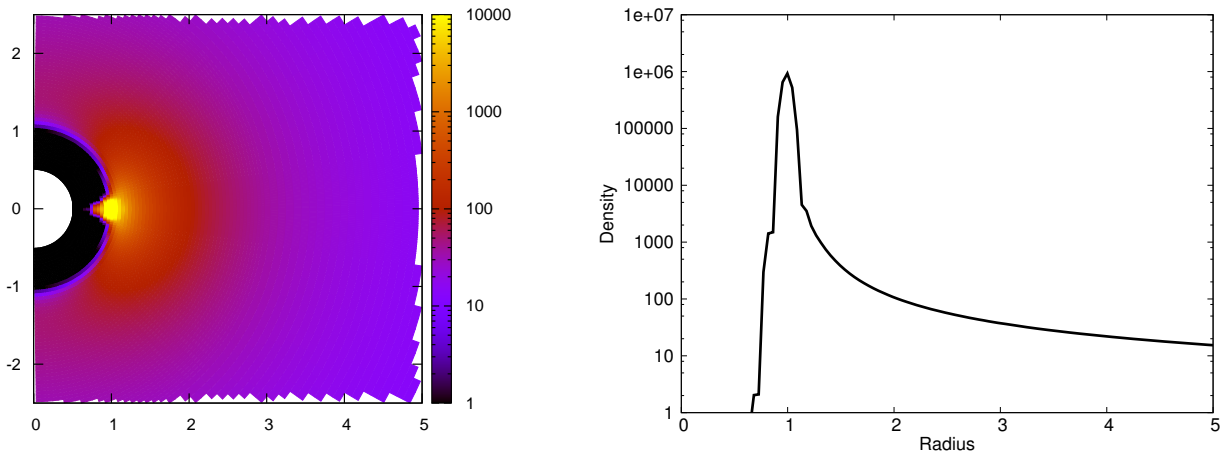


FIG. 2: Left panel: density plot of the accretion flow around a super-spiner with $a = 1.1 M$ (color scheme as described in fig. 1). Right panel: radial density profile on the equatorial plane of the same object. The inner boundary is at $r_{in} = 0.5 M$.

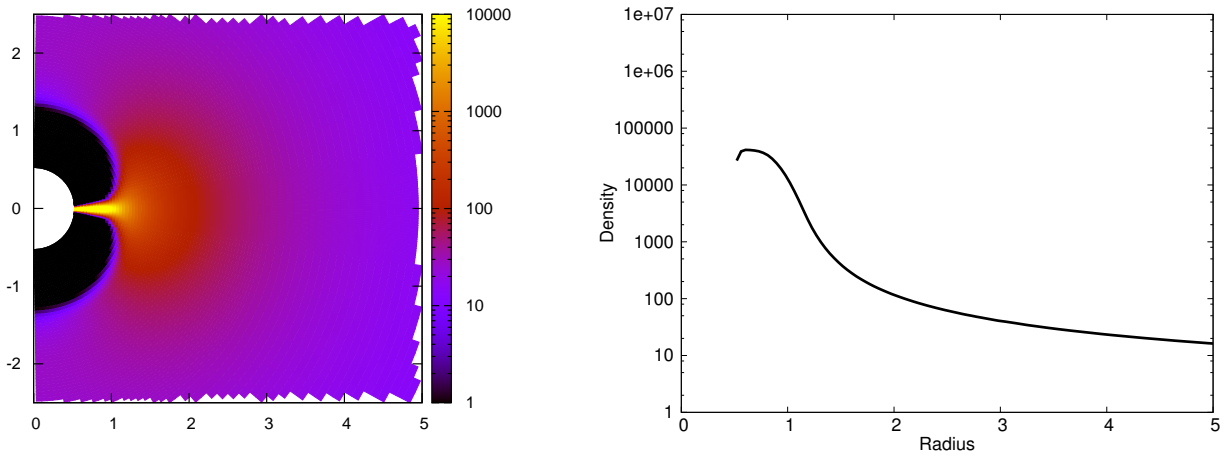


FIG. 3: Left panel: density plot of the accretion flow around a super-spiner with $a = 1.4 M$ (color scheme as described in fig. 1). Right panel: radial density profile on the equatorial plane of the same object. The inner boundary is at $r_{in} = 0.5 M$.

domain of computation (now $r < 0.5 M$). In the right panel, we present the radial density profile on the equatorial plane (i.e. the plane with vertical axis $y = 0$ in the previous plot).

The peculiar feature of the case $a = 1.1 M$ is that the space around the central object is almost empty (the black region in the picture, where actually $\rho \ll \rho_0$). This is not the result of very high inflow velocity of the gas, but the effect of the repulsive force at short distances from the center². The gas around the center is pushed away to larger radii, while the gas far from the object is attracted by the usual gravitational force. The object does not really accrete; instead matter accumulates around it, thus forming a high density cloud. Actually, on the equatorial plane there is some amount of gas falling into the super-spiner, but the fraction of matter with respect to the injected mass is so small that it is negligible. It is therefore clear that we cannot find any quasi-steady state in this case: matter is continuously accumulated into the cloud (fig. 2 shows the density profile at the time $t = 10^4 M$ of the simulation)³.

² Here the repulsive force is due to the singularity; it is not the centrifugal force due to the rotation of the accreting gas. The fact that the gravitational force of a time-like singularity might be repulsive in its neighborhood has been already noticed in the literature, see e.g. refs. [19, 20]. The simplest example is the Schwarzschild spacetime with negative mass: there is no horizon, but a time-like singularity at $r = 0$, and the gravitational force is repulsive, as one can easily see by considering the Newtonian limit.

³ We notice that a similar result was obtained in ref. [21] for the case of Reissner-Nordström naked singularity: even there, no quasi-steady accretion is possible and an “atmosphere” of fluid is formed around the center.

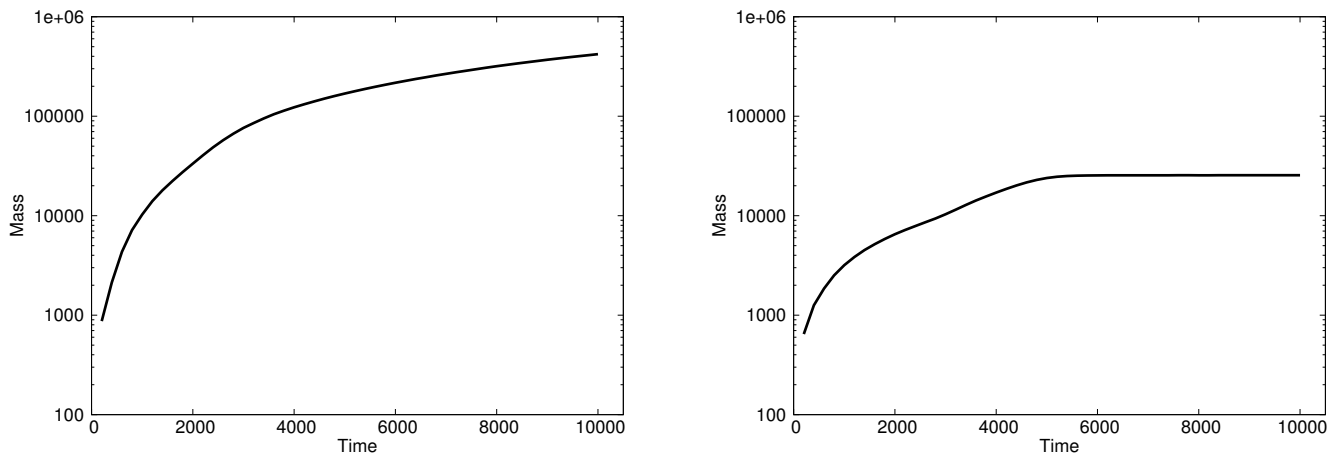


FIG. 4: Rest mass of the gas (in units $M^3 \rho_0$) as a function of time (in units M) inside the region $0.5 M < r < 2.5 M$ in the cases of super-spinars with $a = 1.1 M$ (left panel) and $a = 1.4 M$ (right panel). For values of the Kerr parameter just above the Kerr bound, we do not find any quasi-steady state and the gas is continuously accumulated around the object. For $a = 1.4 M$, the flow reaches a quasi-steady state at $t \approx 6000 M$.

Such a statement is checked by plotting the rest mass of the gas, defined by

$$M_{gas} = \int \rho \sqrt{\gamma} d^3x, \quad (26)$$

in the region $0.5 M < r < 2.5 M$, as a function of time (fig. 4, left panel): as the time goes on, the total mass of the gas increases and there is no quasi-steady state.

As $|a|/M$ increases, more and more matter falls to the center and leaves the domain of computation. The radial coordinate, say r_{max} , of the point of the cloud with the highest density decreases (e.g. $r_{max} \approx 1.0 M$ for $|a|/M = 1.1$, $r_{max} \approx 0.9 M$ for $|a|/M = 1.2$, and $r_{max} \approx 0.8 M$ for $|a|/M = 1.3$) and the growth of the cloud slows down. For $|a|/M = 1.4$ and higher values, the process changes significantly: r_{max} approaches r_{in} and the process reaches a quasi-steady state; that is, the flux leaving the simulation at r_{in} (moving towards the center) equals the flux of matter entering the simulation at $r_{out} = 20 M$. In fig. 3 we can see the density plot of a super-spiner with $a = 1.4 M$. Still there is an empty region (black in the picture) in the neighborhood of the center. However, that is not true near the equatorial plane, where the density increases as r decreases and $r_{max} \approx r_{in}$, see the right panel of fig. 3. The right panel of fig. 4 shows that in this case the accreting flow reaches a quasi-steady state.

Since for $|a|/M \gtrsim 1.4$ the simulations show that r_{max} goes to r_{in} , it is natural to wonder whether the threshold $a = 1.4 M$ dividing two qualitatively different cases is determined by the value of r_{in} . We have therefore run the code with smaller values of r_{in} , finding however the same result: $r_{max} \rightarrow r_{in}$ and for $|a|/M \gtrsim 1.4$ the process can reach a quasi-steady state. Our simulations thus suggest that $|a|/M = 1.4$ is a critical value. We provide a qualitative explanation for the origin of this particular value in the next subsection.

Fig. 5 shows the density plot for more rapidly spinning cases, with $a = 2.0 M$ (left panel) and $a = 3.0 M$ (right panel). The pictures show that the volume of the empty region around the compact object increases for higher values of the Kerr parameter. Yet the accreting matter reaches the inner boundary at r_{in} more and more easily, thus leaving the computational domain and forming a structure similar to a disk. Such a disk is very different from the standard accretion disk around BHs. In very rapid super-spinars, the disk extends from $r \sim |a|/2$ to the center. At smaller radii, the disk becomes thinner and the density of the gas higher. On the other hand, the usual accretion disk around BHs typically ranges from some very large radius, say $\sim 100 M$, inward to $r \sim r_{isco}$, where r_{isco} is the innermost stable circular orbit (ISCO). The latter is $6 M$ for a Schwarzschild BH and as small as M for a BH with $|a|/M = 1$. In addition to this, it is important to notice that here the disk appears in the case of initially spherically symmetric accretion, as the gas initially does not have angular momentum. It is the result of the peculiar gravitational force at small radii around super-spinars.

B. Qualitative Explanation

The results of our simulations may seem too exotic and unexpected. In this subsection, we present a few arguments to show that the emerging picture is physically reasonable.

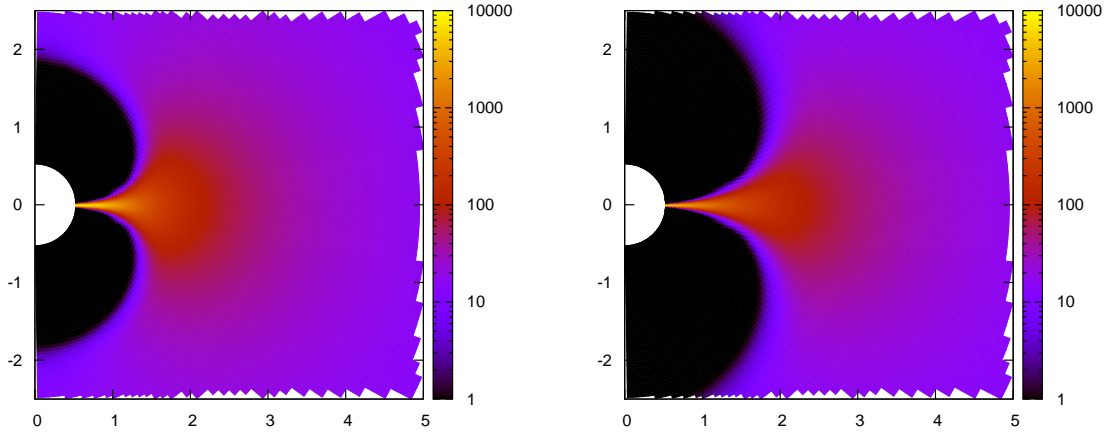


FIG. 5: Density plot of the accretion flow around a super-spinar with $a = 2.0 M$ (left panel) and $a = 3.0 M$ (right panel). Color scheme as described in fig. 1. The inner boundary is at $r_{in} = 0.5 M$.

First, let us see that the effective force can be repulsive at small radii. Assuming negligible velocity (i.e. $\dot{r} \approx \dot{\theta} \approx \dot{\phi} \approx 0$), the radial component of the equations of motion for a massive test particle in Kerr spacetime is

$$\ddot{r} \approx -\Gamma_{tt}^r \dot{t}^2 = -\frac{\Delta M (r^2 - a^2 \cos^2 \theta)}{\varrho^6} \dot{t}^2, \quad (27)$$

where 'dot' stands for a derivative with respect to the affine parameter and Δ is defined in Eq.(18). Since $\Delta > 0$ for any r when $|a| > M$, the force is attractive or repulsive according to the sign of $(r^2 - a^2 \cos^2 \theta)$. The same conclusion can be deduced from the master equations (14): if the fluid is non-relativistic, i.e. $v^2 \ll 1$ and $h \approx 1$, the radial component of eq. (14) becomes

$$\frac{\partial S_r}{\partial t} \approx -\frac{\sqrt{-g}}{\sqrt{\gamma}} \Gamma_{tt}^r T^{tt} g_{rr} = -\frac{\sqrt{-g} M \rho (r^2 - a^2 \cos^2 \theta) \Sigma^2}{\sqrt{\gamma} \varrho^6 \Delta}, \quad (28)$$

and the direction of the force still depends on the sign of $(r^2 - a^2 \cos^2 \theta)$. In the case of Kerr BH with $|a| < M$, the force is always attractive because $(r^2 - a^2 \cos^2 \theta) > 0$ for any $r > r_H > M$, while for $r < r_H$ the Kerr metric does not hold. We note also that, for the case of $r \gg |a|$ and $r \gg M$, eq. (28) reduces to the usual Newtonian case, with $-M\rho/r^2$ on the right hand side.

Eqs. (27) and (28) suggest that the force is repulsive inside the two spherical regions of radius $|a|/2$ and centers with coordinates $r = |a|/2$ and $\theta = 0, \pi$. This is basically the shape and the size of the empty region around the center in the cases $a = 1.4 M$ (fig. 3), $a = 2.0 M$, and $3.0 M$ (fig. 5), while it is less clear for $a = 1.1 M$. According to this interpretation, the origin of the repulsive force at small radii is a pure geometrical effect due to the spin a , and not the result of an effective force due to the angular momentum of the accreting plasma. We checked such a guess by performing some simulations injecting gas with different angular momenta. We found that the shape and the size of the empty regions around the center are essentially unaffected by the choice of the initial angular momentum of the gas, whose effect is instead to make the density profile asymmetric with respect to the equatorial plane.

The origin of the critical value $|a|/M \approx 1.4$ can be understood by slightly improving the previous argument. Since inside the ergoregion everything must rotate, we relax the assumption $\dot{\phi} \approx 0$ and eq. (27) becomes

$$\ddot{r} \approx -\Gamma_{tt}^r \dot{t}^2 - 2\Gamma_{t\phi}^r \dot{t} \dot{\phi} - \Gamma_{\phi\phi}^r \dot{\phi}^2, \quad (29)$$

where

$$\dot{t} = \frac{\Sigma^2 E - 2aMrL_z}{\varrho^2 \Delta}, \quad (30)$$

$$\dot{\phi} = \frac{2aMrE + (\varrho^2 - 2Mr)L_z \csc^2 \theta}{\varrho^2 \Delta}. \quad (31)$$

In order to study the sign of \ddot{r} , we need to specify the constant of motion E and L_z , which are respectively the energy and the angular momentum along the spin (per unit mass) at infinity. For a simple estimate, we can take $E = 1$

(marginally bound orbits) and $L_z = 0$. Generally speaking, the first term on the right hand side of eq. (29) produces an attractive force at large radii and a repulsive force at small radii, while the second and third terms behave in the opposite way; that is, they give a force which is attractive and repulsive respectively for small and large r . It is easy to see that, on the equatorial plane, for $|a|/M$ slightly larger than 1, the force turns out to be attractive at very small and large radii, and repulsive around $r = 0.75 M$. The two values of r , say r_1 and r_2 , for which the force is zero are given by the equation

$$4a^2Mr\Sigma^2 + 4a^2M(r^5 - a^2Mr^2) - \Sigma^4 = 0, \quad (32)$$

where $\Sigma^2 = (r^2 + a^2)^2 - a^2(r^2 - 2Mr + a^2)$. Eq. (32) reduces to the following simple equation

$$a^4 + 2a^2r(r - 2M) + r^4 = 0, \quad (33)$$

which can be seen as a quadratic equation for a^2 , with solution

$$a^2 = r(2M - r) \pm 2r\sqrt{M - r}. \quad (34)$$

As $|a|/M$ increases, the r_1 and r_2 converge to $r = 0.75 M$ and eventually coincide for

$$a_{\text{crit}}/M = \frac{3\sqrt{3}}{4} \approx 1.299, \quad (35)$$

which is the maximum of eq (34). For larger values of the Kerr parameter, eq. (32) has no solutions for $r > 0$ and thus the force is everywhere attractive on the equatorial plane. Such a behavior explains the origin of the critical value separating the two different regimes of accretion found by our numerical study. The small discrepancy between the value obtained in the simulations (about 1.4) and the one obtained analytically (about 1.299) can be easily explained with the difference between the motion of a fluid (for which the hydrodynamical approximation holds, i.e. the mean free path of its particles is much smaller than the characteristic length scale of the system) and the one of a free particle. In particular, the fluid occupies a finite volume and, even if for $|a|/M = 3\sqrt{3}/4$ the force is always attractive on the equatorial plane, that is definitively not true out of the equatorial plane. The result is that there is a sort of bottleneck effect at $r = 0.75 M$ and only when $|a|/M$ is slightly larger than $3\sqrt{3}/4$ all the falling gas can pass this critical point and the process of accretion can reach a quasi-steady state.

IV. ASTROPHYSICAL IMPLICATIONS

Our simulations show that the accretion process onto objects with $|a| < M$ and $|a| > M$ is very different. In the first case, the injected matter is swallowed by the object and the density profile reaches always a quasi-steady configuration: the BH grows at the same rate of the injection of matter. For super-spinars, accretion is more difficult due to a repulsive force in the neighborhood of the center, except near the equatorial plane. Here we can distinguish the cases $|a|/M < 1.4$ and $|a|/M \gtrsim 1.4$. For $|a|$ moderately larger than M , the repulsive force prevents that the accreting gas reaches the central object: the mass of the super-spinner does not increase and the gas is accumulated around the object. A cloud forms and grows; the matter density of this cloud becomes higher and higher. As shown in the left panel of fig. 4, we do not find a quasi-steady state. As the quantity $|a|/M$ increases, more and more of the matter is able to fall all the way into the center. The highest density region of the cloud moves to smaller radii. Then, for $|a|/M \gtrsim 1.4$, the repulsive force in the neighborhood of the center is no longer able to prevent a regular accretion of the super-spinner. The accreting flow can reach a quasi-steady state (see the right panel of fig. 4) by forming a peculiar high density disk on the equatorial plane at very small radii (figs. 3 and 5).

Limiting our considerations to a qualitative level, super-spinars might explain observations like the ones reported in ref. [22]: the blazar PKS 0537-441 produces most of its flux in gamma rays, while for standard accretion onto usual Kerr BH it is not natural to produce gammas more than a few percent in bolometric luminosity [23]. Indeed, if the central object is a BH, one would expect an accretion luminosity proportional to ST^4 , where $S \propto M^2$ is the emitting surface area and T the temperature: a BH does not produce a significant amount of hard radiation. In the case of super-spinars, the temperature of the accreting gas could become higher, because of much higher plasma densities, thus producing harder radiation.

It is however important to bear in mind that *i*) some radiative processes might become important and *ii*) here the accreting matter is modeled as a test fluid. Actually, the particles of the accreting gas can lose energy and angular momentum through some dissipative mechanisms, and that can have some effect on the accretion process, even if we expect that our basic conclusions still hold, especially for small accretion rates. Secondly, the test fluid approximation

breaks down when the mass of the accreting gas is non-negligible in comparison to the original mass of the object, e.g. that is true for super-massive objects at the center of galaxies. For $|a|/M < 1.4$, as the cloud grows, eventually its gravitational field becomes non-negligible, invalidating the test fluid approximation. Here it is difficult to predict what happens only from the present results, but we suggest a few possibilities. For example, the cloud could collapse onto the object, as soon as it wins against the repulsive force around the center. If the accretion rate at large radii is at 10% of the Eddington limit, the mass of the cloud becomes comparable to the mass of the super-spiner after 10^8 yr. The gravitational collapse of the cloud would be likely a violent event, and with two possible results: the formation of a BH with event horizon, i.e. an object with $|a| < M$, or the formation of a heavier super-spiner. The fate of the system presumably depends on the details of the accretion process and of the release of energy and angular momentum during the collapse of the cloud. Another possibility is that an event horizon just forms due to the accumulated matter, hides the mass from outside and no striking radiation is emitted. In the second scenario, the super-spiner would be the first product of the collapse, and then it would evolve into a Kerr BH, presumably without leaving any signature of its previous super-spinning stage.

V. CONCLUSIONS

In this paper we have studied the accretion process onto a spinning object. In particular, we have considered a Kerr spacetime with absolute value of the Kerr parameter a (ratio of spin to mass) either smaller or larger than M , the mass of the object. In the first case, the spacetime contains a BH, in the second one a naked singularity. Our main motivation for considering the possibility of a naked singularity is based on the observation that the singularity is more likely a pathology of classical GR and that in the full theory it must be replaced by something else. We do not know how the central singularity is resolved, but our results are probably not significantly affected by the details of the correct theory. The only relevant quantity astrophysically is likely to be $|a|/M$.

We can distinguish three cases:

1. BHs with $|a|/M < 1$. We find the usual accretion picture: injected matter always reaches a quasi-steady state configuration, in which matter is lost behind the event horizon at the same rate as it enters into the computational domain.
2. Super-spinars with $1 < |a|/M < 1.4$. Here the gas cannot reach the central object, because of a repulsive force in the neighborhood of the center. As a result, the gas is efficiently accumulated around the super-spiner. That leads to the formation and growth of a high density cloud. However, the accumulation process will stop at some point. One possibility is that it is interrupted by violent events due to the gravitational collapse of the cloud onto the object. This could be associated with the formation of a new object, either a BH or a heavier super-spiner. Another possibility is that the accumulated matter creates an event horizon, hiding the object from the outside, and with no abundant release of energy.
3. Super-spinars with $|a|/M \gtrsim 1.4$. Now the repulsive force around the center is no longer capable of preventing a regular accretion of the object. Our simulations find that the flow forms a high density thin disk on the equatorial plane and reaches a quasi-steady state, i.e. matter enters and leaves the computational domain at the same rate. This disk is much closer to the center of the object than in the case of a standard BH.

Acknowledgments

We would like to thank Sergei Blinnikov, Hideki Ishihara, Ken'ichi Nakao, and Lev Titarchuk for useful discussions at different stages of this work. C.B. and N.Y. were supported by World Premier International Research Center Initiative (WPI Initiative), MEXT, Japan. K.F. thanks the DOE and the MCTP at the University of Michigan for support. T.H. was partly supported by the Grant-in-Aid for Scientific Research Fund of the Ministry of Education, Culture, Sports, Science and Technology, Japan (Young Scientists (B) 18740144 and 21740190). R.T. was supported by the Grant-in-Aid for Scientific Research Fund of the Ministry of Education, Culture, Sports, Science and Technology, Japan (Young Scientists (B) 18740144).

[1] Ch. W. Misner, K. S. Thorne and J. A. Wheeler, *Gravitation* (W. H. Freeman and Company, San Francisco, California, 1973).

- [2] A. Lightman, W. H. Press, R. H. Price and S. A. Teukolsky, *Problem Book in Relativity and Gravitation*, (Princeton University Press, Princeton, New Jersey, 1975).
- [3] S. Chandrasekhar, *The Mathematical Theory of Black Holes* (Clarendon Press, Oxford, UK, 1983).
- [4] B. Carter, Phys. Rev. **174**, 1559 (1968).
- [5] R. Penrose, Riv. Nuovo Cim. **1**, 252 (1969) [Gen. Rel. Grav. **34**, 1141 (2002)].
- [6] E. G. Gimon and P. Horava, Phys. Lett. B **672**, 299 (2009) [arXiv:0706.2873 [hep-th]].
- [7] T. Harada and K. i. Nakao, Phys. Rev. D **70**, 041501 (2004) [arXiv:gr-qc/0407034].
- [8] D. C. Robinson, Phys. Rev. Lett. **34**, 905 (1975).
- [9] C. Bambi and K. Freese, Phys. Rev. D **79**, 043002 (2009) [arXiv:0812.1328 [astro-ph]].
- [10] C. Bambi, K. Freese and R. Takahashi, to appear in the *Proceedings of 21st Rencontres de Blois: Windows on the Universe* [arXiv:0908.3238 [astro-ph.HE]].
- [11] S. Doeleman *et al.*, Nature **455**, 78 (2008) [arXiv:0809.2442 [astro-ph]].
- [12] R. Emparan and R. C. Myers, JHEP **0309**, 025 (2003) [arXiv:hep-th/0308056].
- [13] V. Cardoso, P. Pani, M. Cadoni and M. Cavaglia, Class. Quant. Grav. **25**, 195010 (2008) [arXiv:0808.1615 [gr-qc]].
- [14] F. Banyuls, J. A. Font, J. M. Ibanez, J. M. Marti and J. A. Miralles, Astrophys. J. **476**, 221 (1997).
- [15] J. A. Font, Living Rev. Rel. **11**, 7 (2007).
- [16] M. Camenzind, *Compact Objects in Astrophysics: White Dwarfs, Neutron Stars and Black Holes* (Springer-Verlag, Berlin, Germany, 2007).
- [17] A. Mignone, G. Bodo, S. Massaglia, T. Matsakos, O. Tesileanu and C. Zanni, Astrophys. J. Suppl. **170**, 228 (2007) [arXiv:astro-ph/0701854].
- [18] <http://plutocode.to.astro.it/index.html>
- [19] T. Koike, H. Onozawa and M. Siino, arXiv:gr-qc/9312012.
- [20] L. Herrera, Found. Phys. Lett. **18**, 21 (2005) [arXiv:gr-qc/0402052].
- [21] E. Babichev, S. Chernov, V. Dokuchaev and Yu. Eroshenko, arXiv:0806.0916 [gr-qc].
- [22] E. Pian *et al.*, Astron. Astrophys. **392**, 407 (2002) [arXiv:astro-ph/0207355].
- [23] S. Blinnikov, private communication.